

AERODYNAMIC PERFORMANCE OF TWO VERY HIGH LIFT LOW PRESSURE TURBINE AIRFOILS (T106C – T2) AT LOW REYNOLDS AND HIGH MACH NUMBERS

Tony ARTS

von Karman Institute for Fluid Dynamics

Turbomachinery & Propulsion Department – “Jacques Chauvin Laboratory”

72, Chaussée de Waterloo – B1640 Rhode-Saint-Genèse – Belgium

Email : arts@vki.ac.be - <https://www.vki.ac.be/>

Abstract

A detailed experimental analysis of the effects of Reynolds number on the aerodynamic performance of two very high lift low pressure turbine blades (T106C and T2) is presented. The study was held on a large scale linear cascade in the VKI S1/C high-speed wind tunnel operating at fixed high exit Mach number (0.65) and inlet turbulence intensity (0.9 %) with a range of low Reynolds numbers (80,000-250,000). This facility allows an accurate reproduction of the operating conditions encountered in low pressure turbines of modern aero-engines. Aerodynamic upstream and downstream boundary conditions are accurately quantified in order to provide the necessary input for code validation. The two airfoils are characterized by a high pitch-to-chord ratio, implying a significant diffusion, and therefore risk of separation, along their rear suction side. Besides the investigation conducted for steady, uniform inlet conditions, the simulation of incoming periodic passing wakes was also realized. Depending on the operating Reynolds number, the rear suction side flow is characterized by a more or less important (short or long) separation bubble. The bursting phenomenon of the bubble is clearly demonstrated. The control of the separation is tentatively addressed by means of passive local roughness. Its effect on loss performance is also demonstrated. Besides the knowledge gained on unsteady transition and separation phenomena in low pressure turbines operated at engine similar operating conditions, the large variety of boundary conditions also provides a unique database for code validation dealing with separated flow transition at high Mach number and low Reynolds number in turbomachinery.

1. Introduction

The demand for higher bypass ratios in modern commercial jet engines requires low pressure turbines to provide an increasingly larger power output allowing the drive of large fans without penalizing the efficiency. At the same time, their design asks for a reduction of the turbine blade count, in order to save weight and secure lower manufacturing and operating costs. This implies an increase of the aerodynamic load on each blade, towards the development of very high lift airfoils. The latter are characterized by a high velocity peak on the suction side, followed by a significant diffusion. The resulting strong adverse pressure gradient along this surface may possibly induce a separation of the boundary layer, particularly at low Reynolds number, which causes a significant loss in lift and a consequent drop in engine efficiency (Mayle, [1]). For large commercial turbofans, a loss in LP turbine efficiency of the order of 2 % may occur between sea-level take-off conditions (Volino and Hultgren, [2]), where the Reynolds number in the LP turbine is typically around $5 \cdot 10^5$, and high-altitude cruise flight, where Re is about $5 \cdot 10^4$ (Hodson and Howell, [3]). Curtis et al. [4] showed that the suction side boundary layer is the primary source of losses in the LP turbine, with the eventual separation bubble causing the main detrimental effect. Consequently, analyzing and predicting the evolution of the suction side boundary layer is of utmost importance to improve engine design.

Due to the low cruise Reynolds number conditions, a large part of the boundary layer around LP turbine blades may be transitional (Mayle, [1]). Since turbulent flows are much more resistant to separation than laminar ones, the precise prediction of transition development is particularly vital in the case of very high lift airfoils, for which the high initial acceleration tends to keep the suction side boundary layer laminar until the velocity peak even in presence of significant free-stream turbulence intensity. If the following diffusion is strong enough, a laminar boundary layer is not able to withstand the resulting adverse pressure gradient and separates from the blade surface. Volino [5] observed that, in this kind of situation, a laminar boundary layer is likely to separate just after the suction peak. However, if transition occurs soon enough in the separated shear layer, the flow will reattach. Transition and separation are thus linked.

Mayle [1] classified three modes of transition: natural transition, initiated by Tollmien-Schlichting waves typical of attached, very low turbulence flows; bypass transition, caused mainly by high free-stream turbulence intensity; separated flow transition, which takes place in the shear layer over a separation bubble. He considered the last mode to be by far the most important for LP turbine applications. He also classified the separation bubbles in two different types, long or short, basing the distinction on the bubble effect on the global pressure distribution along the suction

side, rather than on the physical length of the bubble. While long bubbles are associated with a significantly modified pressure distribution, high losses and reduction of the exit flow angle, short bubbles have only a local effect and, away from them, the pressure distribution is close to the one predicted without any separation. Therefore, short bubbles can be an effective way to force the transition of the boundary layer and to avoid loss augmentation. The change in the bubble type, from short to long, is called bursting. It is an unsteady process which can be triggered even by small changes in either the Reynolds number or the angle of attack. Mayle [1] claimed that the topological difference between short and long bubbles is not the length of the transition, which is independent on the type of bubble, but rather the length of the unstable laminar shear layer. He also provided a prediction model based on the assumption that the separated flow transition ends at the reattachment point, whereas Walker [6] pointed out that the flow may still be transitional at the reattachment and that the end of transition may occur well after the pressure recovery process is completed.

Hatman and Wang [7, 8, 9] confirmed Walker's statement after performing low speed experiments on a flat plate at low turbulence intensity and constant adverse pressure gradient. They considered separated flow transition as the result of the superposition of two types of instabilities: the Tollmien-Schlichting viscous instability and the Kelvin-Helmholtz inviscid instability. They described three different types of separation bubbles: short bubbles with transitional separation, short bubbles and long bubbles, both of the laminar separation type. The predominance of one type of instability determines the mode of transition and thus the type of the bubble. Houtermans et al. [11], also supported the findings of Volino [10] after obtaining results in good agreement with those described by Hatman and Wang.

The aerodynamic performance of two very high lift low pressure turbine (LPT) airfoils (T106C and T2) was experimentally investigated at the von Karman Institute (Jacques Chauvin Laboratory). The main objective of this study was to quantify the effects of artificial roughness and incoming wakes at low free-stream Reynolds numbers and engine representative exit Mach numbers. The background free-stream turbulence was kept low (0.9 %). Both airfoils were tested in a linear cascade configuration. The first one is based on the well-known T106 profile, already extensively investigated at the University of Armed Forces in Munich (Germany). The second one contains a new profile (T2), designed at the VKI.

2. Experimental Apparatus

The measurements were conducted in the high speed, low Reynolds facility S1/C of the von Karman Institute. It is a continuous closed circuit facility driven by a 615 kW axial flow compressor. A cooler allows maintaining the temperature at near atmospheric condition (293 K) and a dry air is maintained at all conditions. The mass flow can be regulated via a by-pass valve. A vacuum pump allows lowering the tunnel absolute pressure to $\sim 10,000$ Pascal. This wind tunnel was originally designed for the study of laminar shock boundary layer interactions and various supersonic flow configurations. It was modified into a turbomachinery cascade tunnel by replacing the first elbow (upper left elbow in Fig. 1) following the diffuser by a cascade test section. The cylindrical rear part of the diffuser is assigned the role of a settling chamber for the cascade test section. It is fitted with wire meshes and honeycombs to ensure homogeneous flow conditions.

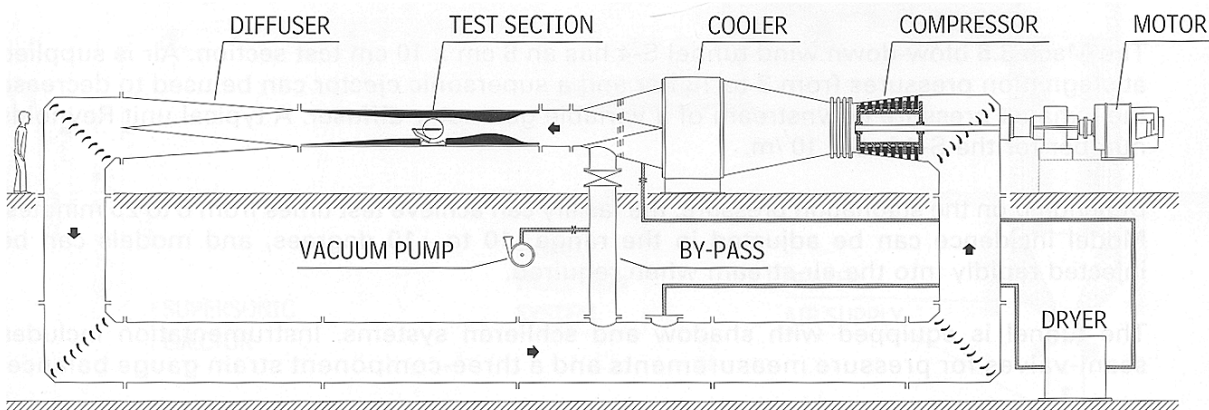


Fig. 1 – S1/C wind tunnel circuit

A sketch and a picture of the cascade model are shown in Figs. 2a and 2b. Vertical and lateral contractions provide the transition between the original circular parts of the wind tunnel and the cascade. The latter entrance height can be varied between 375 and 650 mm. The span is 225 mm, which guarantees a sufficiently high aspect ratio and therefore limits the impact of the endwall boundary layers on the central part of the channel. The linear cascade ensemble is made up of 6 to 9 full blades plus two end-blocs at the extremities of the cascade, shaped respectively according to the pressure and suction side profiles of normal blades (Fig. 2a). The cascade is mounted into two large circular side walls

(1,120 mm diameter) allowing a continuous change of the inlet flow angle. Upstream passive grids can also vary the global free-stream turbulence intensity, but this will not be discussed in the present paper.

To simulate the blade row interference effects due to wake blade interactions, the test section is equipped with a upstream high speed rotating bar system (Figs. 3a and 3b). The wake generator consists of a disc of 625 mm diameter equipped for the present investigation with 32 bars of 2 mm diameter and 215 mm length, made of molybdenum. The rotating bars are only parallel to the blade leading edge when passing in front of the central blade. In this position the bars extend over the entire blade span except for a clearance of 30 mm to the opposite wall for safety (and two earlier failures) reasons. Leakage flows at the passage of the bars through the upper and lower tunnel walls are minimized by sealed cavities. The generator is lodged in a large semi-circular housing mounted on the circular cascade side wall. The wake generator is driven by a 3 kW electric motor up to 3000 rpm which corresponds to a bar passing velocity at blade mid-span of ~ 140 m/s, providing therefore a correct flow coefficient. The generator is brought to nominal rpm, at the lowest local pressure conditions, before starting the main flow.

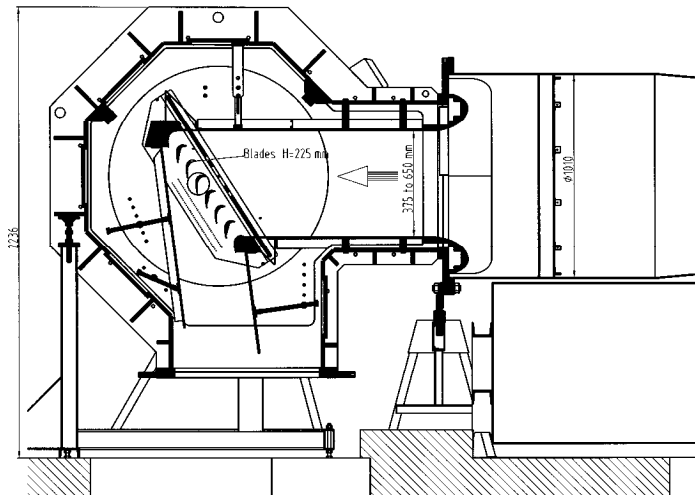


Fig. 2a – Sketch of the cascade



Fig. 2b – Assembly of the cascade model

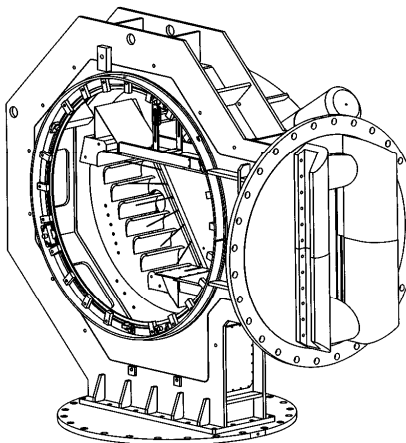


Fig. 3a – Rotating upstream bars

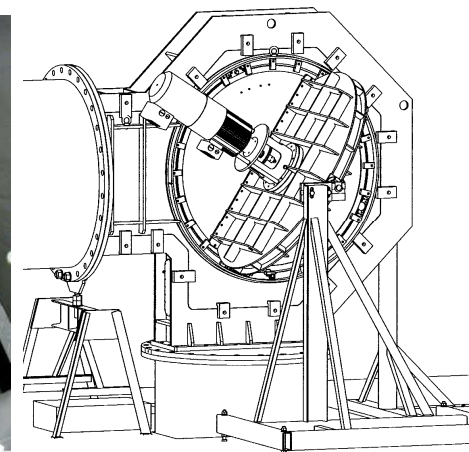


Fig. 3b – Drive of the wake generator

Instrumentation

The central blade of the cascade is alternatively instrumented with wall pneumatic pressure taps, fast response wall pressure sensors and hot film gauges. There is a dense instrumentation concentration in the area of expected boundary layer separation at low Reynolds numbers. The inlet boundary conditions are accurately quantified by pneumatic wall static pressure taps and 3 hole pressure probes as well as a fast response pressure probe and a crossed hot wire probe (for the incoming wakes) whereas pneumatic wall static pressure taps and a 5 hole pneumatic pressure probe (diameter of 3.2 mm) accurately measures the downstream wake and deviation.

Blade and cascade characteristics

The T106C and T2 blade and cascade geometries are presented in the following table and in Fig. 4.

	T106C	T2
Chord length (mm)	93.01	96.35
Blade height (mm)	225.0	225.0
Aspect ratio	2.4	2.34
Pitch-to-chord ratio	0.95	1.05
Throat (mm)	43.38	50.99
Stagger angle (deg)	30.71	33.53
Arc \cos (throat/pitch) (deg)	60.58	59.74
Inlet flow angle	32.7	32.7
Exit Mach number	0.65	0.65

Table 1 – Cascade and airfoil characteristics

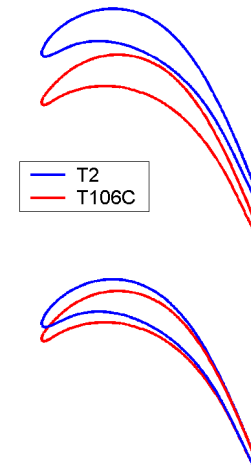


Fig. 4 – Cascade geometries

Local roughness

The present study also includes the impact of a localized roughness element on the suction side in order to possibly control, in a passive way, an early transition of the boundary layer before separation. The roughness element is a wavy metal sheet of 2 mm width and 0.2 mm thickness. The position of the blade roughness element on the suction side was chosen as a result from the velocity distributions measured along the smooth profile. It was finally decided to place the roughness element just upstream of the separation bubble identified at the lowest tested Reynolds number. This position corresponds to $x/c_{ax} = 0.664-0.705$ for the T106C airfoil and $0.366-0.431$ for the T2 airfoil (indeed far more upstream).

3. Steady State Performance Results

The evolution of the velocity distribution along the axial chord for the T106C and T2 blades is depicted on Figs. 5a and 5b for three exit isentropic Reynolds numbers (based on blade chord) (80,000 – 140,000 and 250,000 for T106C and 100,000 – 185,000 and 250,000 for T2) at the nominal outlet Mach number (0.65). A fully turbulent prediction using Prof. Arnone's TRAF code (Arnone [12]) is also provided. Considering T106C, at the lowest Reynolds number, the separation bubble can be considered as long (as can also be seen from the loss and exit angle information). Therefore it has a strong influence on the velocity peak level, on the rear suction side value and on the performance. As the Reynolds number increases, the physical length of the bubble reduces. The separation point moves downstream and doesn't change that much with the Reynolds number. The velocity peak is higher, the rear velocity distribution is closer to the one predicted by the turbulent numerical simulations and therefore, the influence on the performance is reduced. Considering the T2 cascade, the flow appears to suffer from much more severe separations. The separation extends almost until the trailing edge for Reynolds number values up to 160,000 (all results not shown). At the highest Reynolds number value (250,000), a separation bubble still exists, extending from x/c_{ax} values ranging between about 0.73 and 0.85. The flow remains completely separated until the trailing edge for the lowest Reynolds number values. For the highest Reynolds number values, the physical length of the bubble reduces; the rear velocity distribution is closer to the one predicted by turbulent numerical simulations and therefore, the influence on the performance must be reduced.

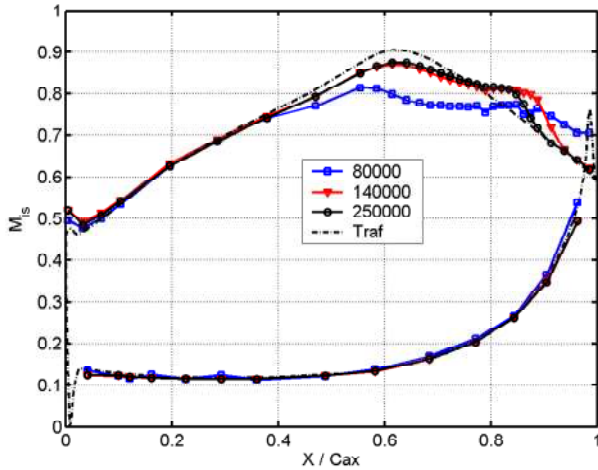


Fig. 5a – “smooth” T106C blade velocity distribution

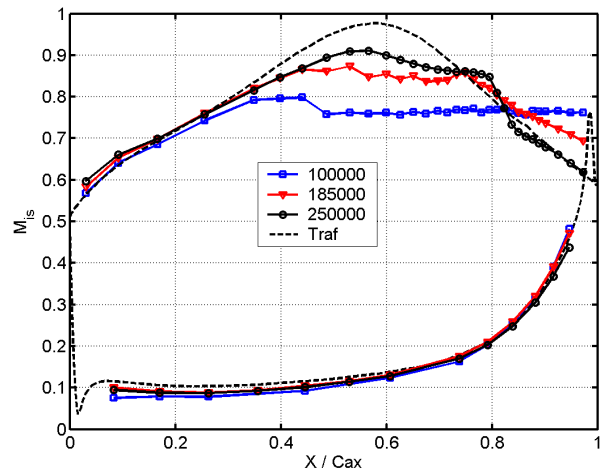


Fig. 5b – “smooth” T2 blade velocity distribution

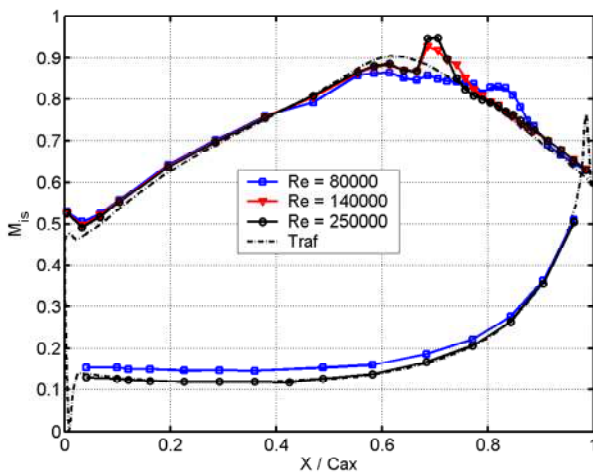


Fig. 6a – “rough” T106C blade velocity distribution

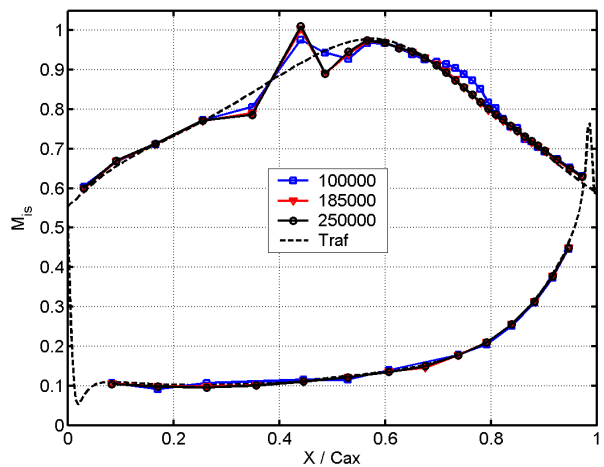


Fig. 6b – “rough” T2 blade velocity distribution

Fig. 6a shows the evolution of the isentropic Mach number along the “rough” T106C blade. At the two highest Reynolds numbers, the presence of the roughness induces an over-speed. The local roughness induces a separation of the boundary layer that reattaches after a short distance. The boundary layer is now able to withstand the adverse pressure gradient without separation. The shorter is the distance, the lower is the interaction with the free-stream flow and so the influence on the performance. At lower Reynolds number, the boundary layer separates before the separation. However, the presence of the local roughness seems to promote the transition in such a way that the free shear layer reattaches to the blade before the trailing edge. The bubble can here be considered as short which is the opposite situation to the one encountered for the smooth airfoil. This behavior explains the gain in performance at this low Reynolds number. The corresponding results on the “rough” T2 airfoil are presented in Fig. 6b. For all tested Reynolds numbers, the presence of the roughness again induces a local over-speed, eventually slightly above the sonic level. This roughness element induces a separation of the boundary layer; the latter reattaches to the blade. The boundary layer is now able to better withstand the stronger adverse pressure gradient. For the lower Reynolds numbers, the boundary layer still shows a small separation along the rear part of the suction side. However, due to its presence, the local roughness seems to promote the transition in such a way that the free shear layer reattaches to the blade. The bubble can be here again considered as short. This behaviour explains the gain in performance at this low Reynolds numbers.

Similar information is retrieved from the hot films. The latter provide a time-resolved “pseudo-shear stress”. The analysis of the time-averaged and RMS results allow complementing the analysis of the onset, development and possible reattachment of the rear suction side separation bubble. Figs. 7a and 7b present this information for the “smooth” T106C profile. The abscissa is drawn along the axial chord. Fig. 7a clearly shows the growing extension of the separation bubble when reducing the exit Reynolds number, with a clear open separation at the lowest value of Re. This information, together with the wall isentropic Mach number distribution, allows establishing a rather precise determination of separation- transition onset and end. Similar information is of course available for the T2 cascade.

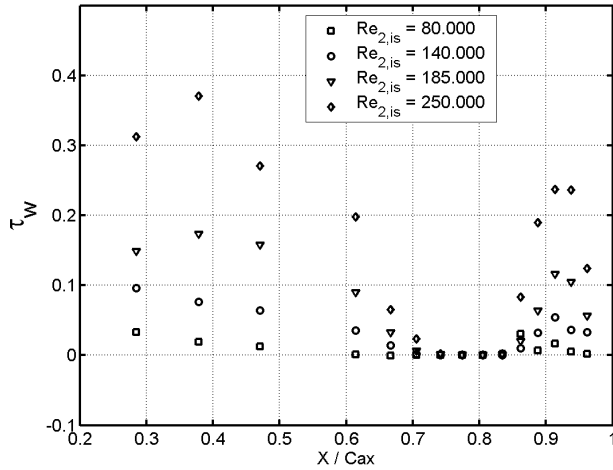


Fig. 7a – “smooth” T106C mean pseudo shear stress

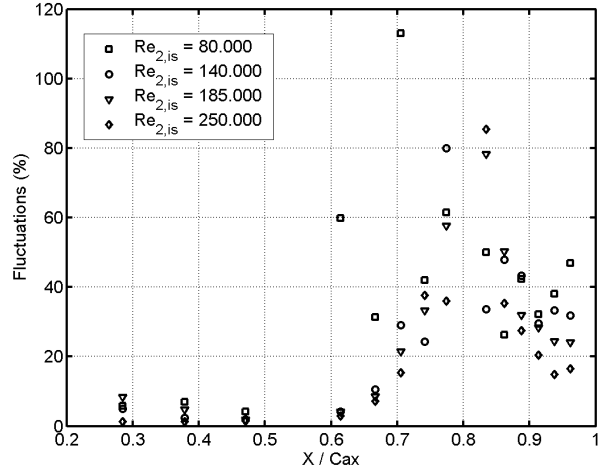


Fig. 7b – “smooth” T106C RMS pseudo shear stress

The mass averaged kinetic energy loss coefficient evolutions of both cascades are presented in Figs. 8a and 8b in function of the isentropic exit Reynolds number (based on blade chord). This loss coefficient is defined as:

$$\zeta = 1 - \frac{1 - \left(\frac{\overline{P_2}}{\overline{P_{02}}}\right)^{\frac{\gamma-1}{\gamma}}}{1 - \left(\frac{\overline{P_2}}{\overline{P_{01}}}\right)^{\frac{\gamma-1}{\gamma}}}$$

The over-bar values are mass-averaged over one pitch. These figures present a summary of all investigated cases. Detailed wake profiles were measured, but not shown here. The impact of the suction side separation bubble along the “smooth” suction sides in function of exit isentropic Reynolds number is clearly seen.

So far, we will consider the steady state (smooth and rough) cases. The steady “smooth” results translate, in terms of performance, what was already known from the blade velocity distributions. The long bubbles seen at low Reynolds number induce high losses. The impact of the local roughness, in promoting an early transition, is more than significant at low Reynolds number for the T106C airfoil and along the full Reynolds number range for the T2 profile.

Similar conclusions are drawn from the exit angle distributions, both in terms of global performance and bubble size. The results are not shown here because of a lack of space, but are available upon request.

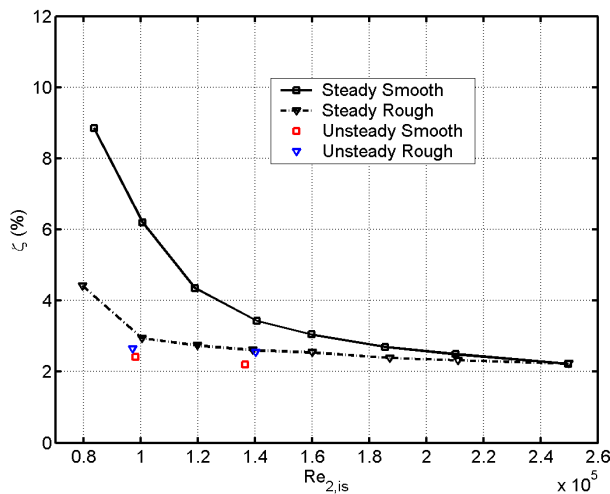


Fig. 8a – T106C kinetic energy loss evolution (all configurations)

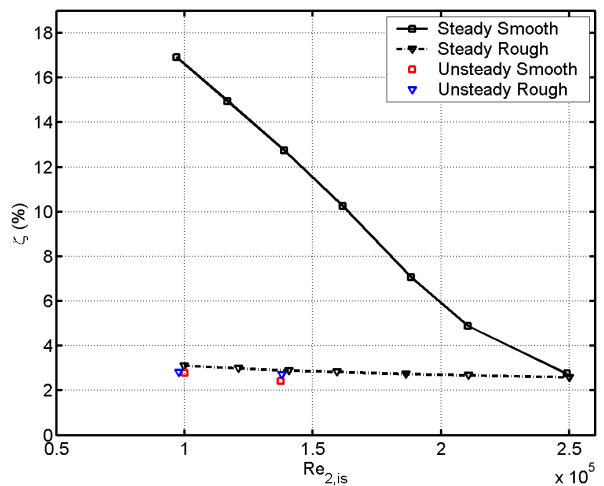


Fig. 8b – T2 kinetic energy loss evolution (all configurations)

4. Performance Results under the Presence of Periodic Incoming Wakes

Inlet total pressure

The total pressure downstream of the wake generator was measured by means of a fast response total pressure probe. This characterization was done at two exit isentropic Reynolds number values (100,000 and 140,000). The upstream wake profile changes with respect to its relative position to the airfoil (upstream potential effect). The relative variations are quantified in Fig. 9a. The two wake profiles plotted in this figure represent two evolutions at two different pitch-wise positions in the measurement plane upstream of the leading edge. The maximum wake depth ($\Delta P1$) amounts to 494 Pascal (5.63 % of P_{01}) at $Re = 100,000$ and 727 Pascal (5.87 % of P_{01}) at $Re = 140,000$. Depending upon the evaluation location, the maximum potential effect (i.e. the variation in wake depth, or $\Delta P2$) amounts to 134 Pascal (1.5 % of P_{01}) at $Re = 100,000$ and 188 Pascal (1.5 % of P_{01}) at $Re = 140,000$.

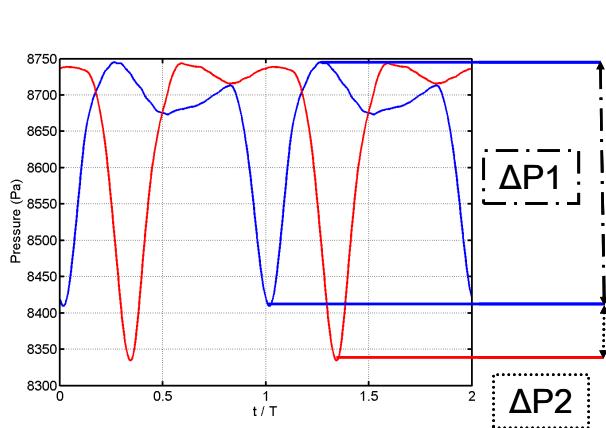


Fig. 9a – Inlet/Exit total pressure variations

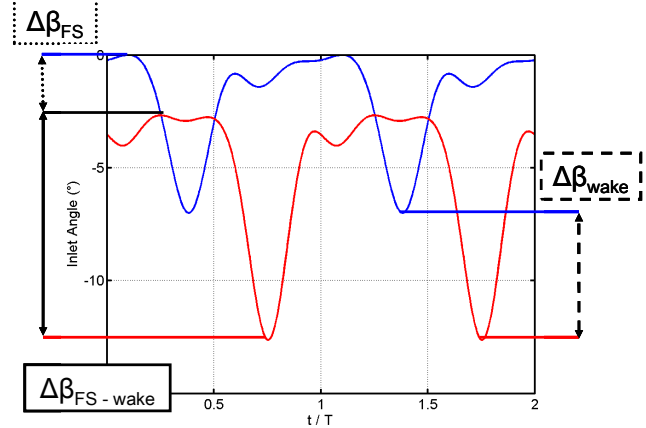


Fig. 9b – Inlet/Exit total pressure variations

Inlet flow angle

The relative inlet flow angle evolution downstream of the periodic wake generator was measured by means of a crossed hot wire probe. This characterization was also done at two Reynolds number values (100,000 and 140,000). Because of the same potential flow effect, the upstream angle profile changes with respect to its relative position to the airfoil. The relative variations are quantified in Fig. 9b. The two profiles plotted in this figure represent two evolutions at two different pitch-wise positions in the measurement plane upstream of the leading edge. The three quantities of interest are $(\Delta\beta_{FS})_{max}$ representing the maximum difference in free-stream angle due to the upstream potential effect of the cascade 2.97 deg at $Re = 100,000$ and 2.94 deg at $Re = 140,000$), $(\Delta\beta_{wake})_{max}$ representing the maximum angle difference in the wake due to the upstream potential effect of the cascade (6.56 deg at $Re = 100,000$ and 6.81 deg at $Re = 140,000$) and $\Delta\beta_{FS-wake}$ representing the difference between the free-stream and the wake (5,48-10 deg at $Re = 100,000$ and 7-11.7 deg at $Re = 140,000$).

Upstream velocity and turbulence intensity

Combining all upstream measurements led to the non dimensional velocity and turbulence profiles presented in Figs. 10a and 10b. The abscissa is the non dimensional time between the passage of two bars. The free-stream turbulence (between wakes) is 0.9 %. In the wake, the turbulence increases to values up to 16 ... 17 %. The values are plotted for two exit isentropic Reynolds number values.

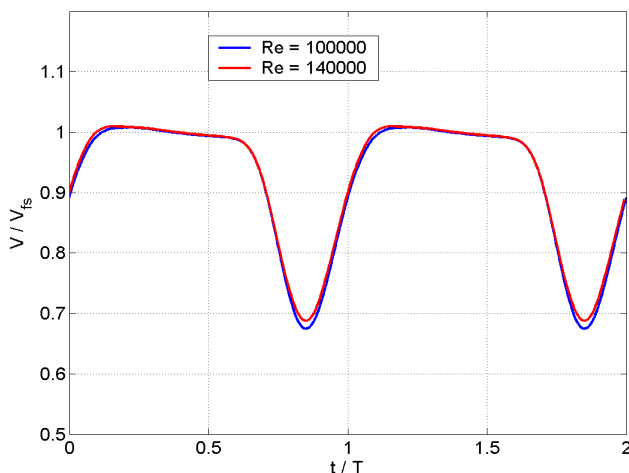


Fig. 10a – Upstream velocity profile (incoming wakes)

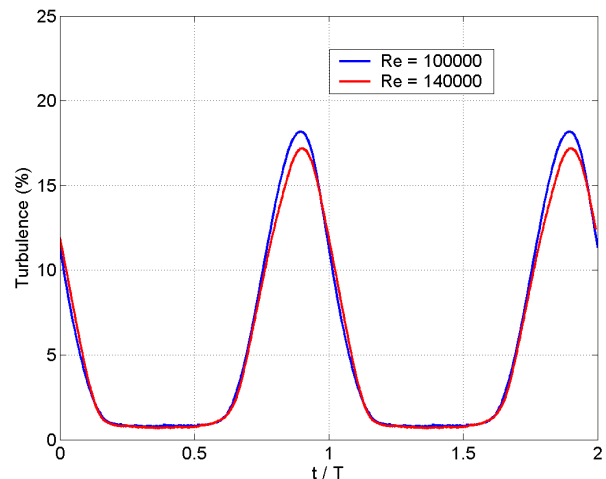


Fig. 10b – Upstream turbulence intensity profile (incoming wakes)

Blade velocity distribution

The evolution of the velocity distribution along the suction side of the “smooth” T106C and T2 blades is shown in Figs. 11a and 11b for an exit Reynolds number value of 100,000. The isentropic exit Mach number value is equal to 0.65. The dashed line represents the results (M_{is}) obtained from a steady state (uniform upstream conditions, no wakes simulated) Navier-Stokes prediction (fully turbulent – Baldwin Lomax model – TRAF code). The blue line and symbols correspond to the results (M_{is}) obtained in absence of the wake generator, the red line and symbols correspond to the measurements (M_{is}) obtained from the same pneumatic taps, but with the wake generator in operation. The green and purple lines and symbols provide respectively the maximum and minimum envelope of the isentropic Mach number as determined from the fast response pressure sensors over one period after a phase-locked average of the signal over about 1000 events. The modification (and reduction) of the separation phenomenon is clearly put in evidence.

For the T2 profile, from the pneumatic surface pressure measurements, a “mean” bubble still exists between $X/C_{ax} \approx 0.70$ and 0.85 . The maximum envelope shows a strong peak at $X/C_{ax} \approx 0.75$, where sonic conditions are reached. This points to the existence of a small local unsteady shock wave, with consequences on the losses.

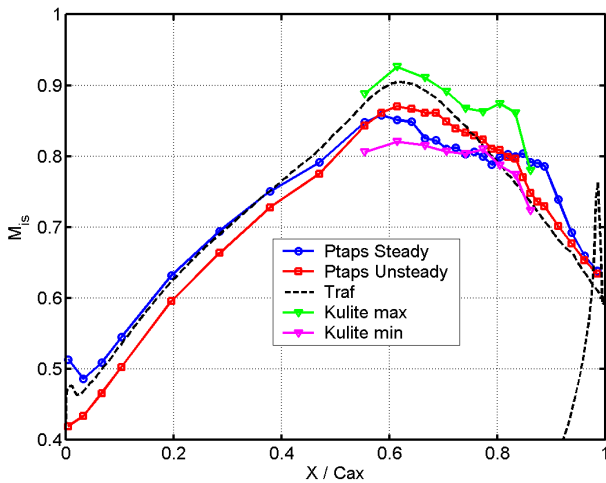


Fig. 11a – Blade velocity distribution T106C (incoming wakes – phase lock average)

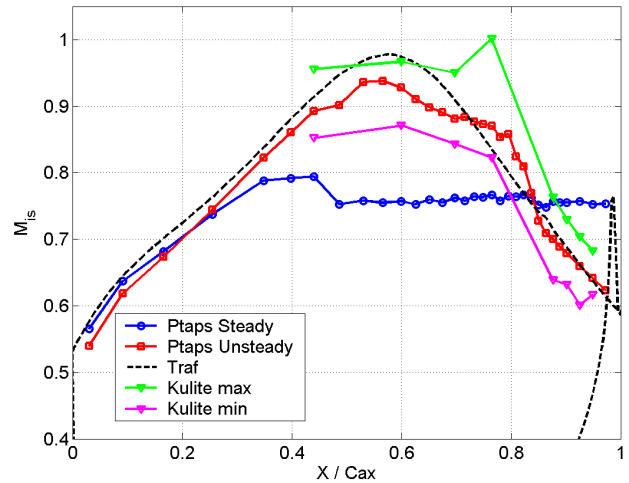


Fig. 11b – Blade velocity distribution T2 (incoming wakes – phase lock average)

The availability of the fast response pressure transducers also allowed building space-time diagrams for the isentropic wall Mach number. The results were phase-lock averaged for this purpose. The resulting phase-lock isentropic Mach number contours and their RMS are presented in Figs. 12a and 12b for the “smooth” T106C cascade. The abscissa is drawn along the axial chord and the ordinate is the reduced time between two successive wakes. The unsteady character of the velocity, and therefore of the separation bubble (moving back and forth) also appears clearly from these results.

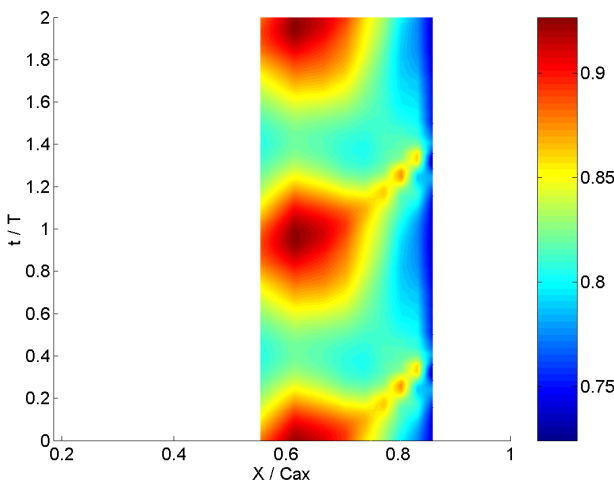


Fig. 12a – Periodic wall isentropic Mach number - T106C (incoming wakes – phase locked average)

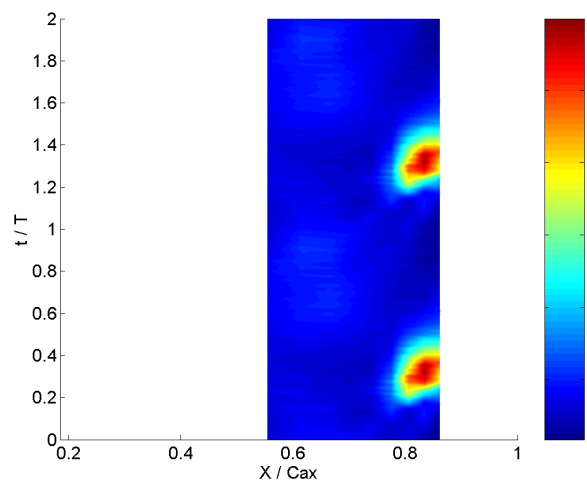


Fig. 12b – RMS – T106C (incoming wakes – phase locked average)

The pseudo shear stresses were obtained along the suction side from an array of hot films. The results (again expressed under the form of space-time diagrams) obtained for an exit Reynolds number value of 100,000 are presented in Figs. 13a and 13b. The isentropic exit Mach number value is again equal to 0.65.

Similar results are of course available for the second isentropic Reynolds number as well as for the T2 cascade. A similar investigation was done for the “rough” profile. A sample of these results, obtained at an exit isentropic Reynolds number value of 100,000 is presented in Figs 14 a-d and 15 a-d. The abscissa is measured along the axial chord and these figures present the beneficial effects of local roughness on the pseudo wall shear stress for the T106C and T2 cascades.

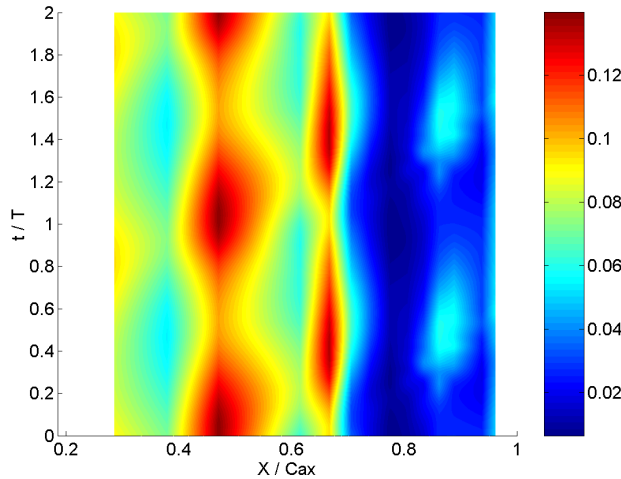


Fig. 13a – Periodic wall pseudo shear stress - T106C (smooth blade – incoming wakes – phase locked data)

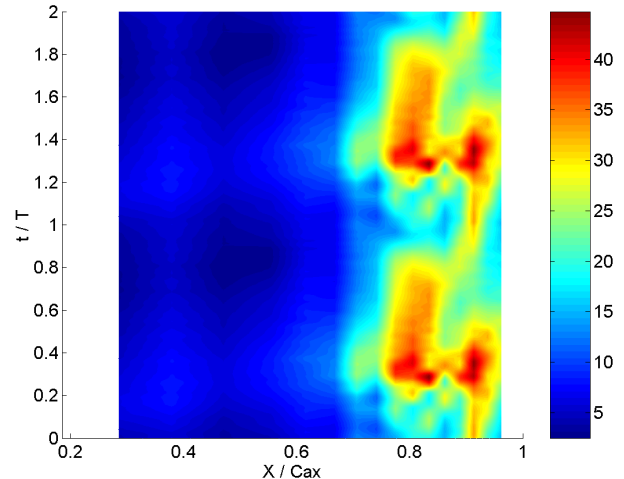


Fig. 13b – RMS – T106C (smooth blade – incoming wakes – phase locked data)

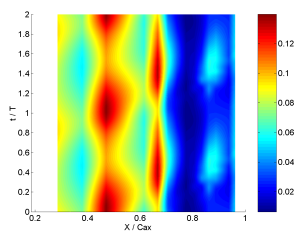


Fig. 14a – Mean τ_w (T106C) (Smooth blade)

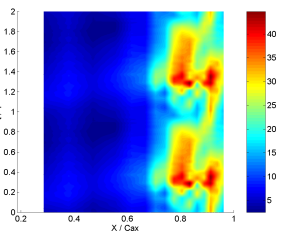


Fig. 14b – RMS τ_w (T106C) (Smooth blade)

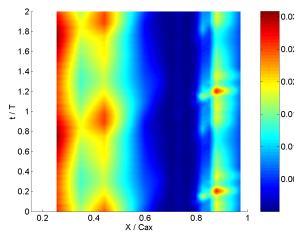


Fig. 14c – Mean τ_w (T2) (Smooth blade)

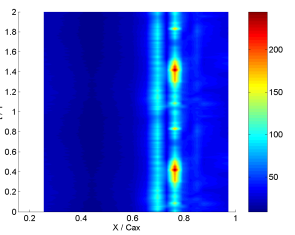


Fig. 14d – RMS τ_w (T2) (Smooth blade)

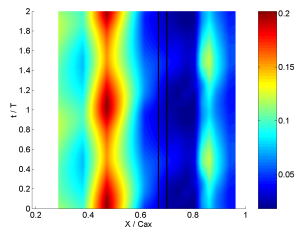


Fig. 15a – Mean τ_w (T106C) (Rough blade)

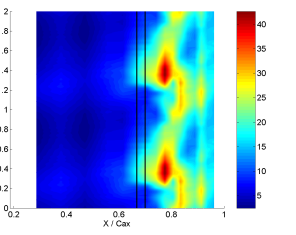


Fig. 15b – RMS τ_w (T106C) (Rough blade)

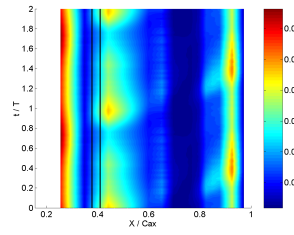


Fig. 15c – Mean τ_w (T2) (Rough blade)

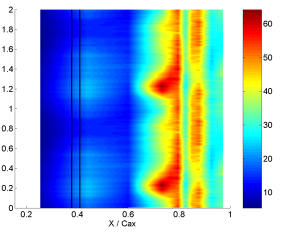


Fig. 15d – RMS τ_w (T2) (Rough blade)

The global aerodynamic performance of both cascades (T106C and T2), expressed in terms of kinetic energy loss coefficient, is shown in Figs. 7a and 7b (unsteady results). From those results, it appears that, for a smooth profile, the incoming wakes are as efficient as a local roughness to reduce the loss at low Reynolds number (i.e. to “kill” most of the laminar separation bubble). The combination of incoming wakes and local roughness does not seem to bring a significant improvement.

5. Conclusions

The present contribution focused on the evaluation and comparison of the aerodynamic performance of two high lift low pressure turbine blades (T106C and T2, the latter being designed at the von Karman Institute). The effects of the introduction of local roughness (upstream of the velocity peak along the suction side) and/or incoming periodic wakes (generated by upstream high speed rotating bars) were carefully measured and analysed. Several measurement techniques, such as pneumatic and time resolved wall static pressure, pseudo skin friction and downstream kinematic loss coefficient (via a total pressure measurement) provided the basis for an in-depth comparison between the two cascade geometries, operated within a large range of Reynolds number, at low free-stream inlet turbulence. The latter

parameter remains of course of importance in a further evaluation of both cascades performance. The present results clearly show a significant influence from either the local roughness or the incoming wakes. The combination of both effects does not seem to bring a further, significant benefit.

In addition to a careful and in-depth analysis of the flow phenomena, the present study aims at providing detailed, precise, well-resolved and well-supported support for code validation.

Acknowledgements

The experimental work described in this paper was performed within the European research project UTAT “Unsteady Transitional Flows in Axial Turbomachines” G4RD-CT-2001-00628. The author also acknowledges the contributions of Prof. C.H. Sieverding in the design and commissioning of the facility as well as of Mr R. Houtermans in the experimental programme.

References

- [1] Mayle R. E., 1991, “The Role of Laminar-Turbulent Transition in Gas Turbine Engines”, ASME J. of Turbomachinery, **113**, pp. 509-537.
- [2] Volino R. J., Hultgren L. S., 2001, “Measurements in Separated and Transitional Boundary Layers Under Low-Pressure Turbine Airfoil Conditions”, ASME J. of Turbomachinery., **123**, pp. 189-197.
- [3] Hodson H. P., Howell R. J., 2005, “The role of transition in high-lift low-pressure turbines for aeroengines”, Progress in Aerospace Sciences 41 (2005), pp. 419-454.
- [4] Curtis E. M., Hodson H. P., Baniaghbal M. R., Denton J. D., Howell R. J., Harvey N. W., 1997, “Development of Blade Profiles for Low-Pressure Turbine Applications”, ASME J. of Turbomachinery., **119**, pp. 531-538.
- [5] Volino R. J., 2002, “Separated Flow Transition under Simulated Low-Pressure Turbine Airfoil Conditions: Part 1-Mean Flow and Turbulence Statistics”, ASME J. of Turbomachinery, **124**, pp. 645-655.
- [6] Walker G. J., 1993, “The Role of Laminar-Turbulent Transition in Gas Turbine Engines: A Discussion”, ASME J. Turbomach., **115**, pp. 207-217.
- [7] Hatman, A, Wang, T., 1998, “Separated Flow Transition. Part 1-Experimental Methodology and Mode Classification”, ASME Paper 98-GT-461
- [8] Hatman, A, Wang, T., 1998, “Separated Flow Transition. Part 2-Experimental Results”, ASME Paper 98-GT-462
- [9] Hatman, A, Wang, T., 1998, “Separated Flow Transition. Part 3-Primary Modes and Vortex Dynamics”, ASME Paper 98-GT-463
- [10] Volino R. J., 2002, “Separated Flow Transition Under Simulated Low-Pressure Turbine Airfoil Conditions: Part 2-Turbulence Spectra”, ASME J. Turbomach., **124**, pp. 656-664
- [11] Houtermans, R., Coton, T., Arts, T., 2004, “Aerodynamic Performance of a Very High-Lift Low Pressure Turbine Blade with Emphasis on Separation Prediction”, J. of Turbomachinery, **126**, pp 406-413.
- [12] Arnone, A., 1994, “Viscous analysis of a three-dimensional rotor flow using a multigrid method”, ASME J. of Turbomachinery, **116**, pp 435-445